2 The Random Phase Approximation and its Applications to Real Materials

Xinguo Ren

CAS Key Laboratory of Quantum Information

University of Science and Technology of China

Jinzhai Road 96, Hefei

Contents

1   Introduction

The random phase approximation (RPA) is a fundamental concept that plays a central role in many-body physics. The concept was developed by Bohm and Pines [1,2] in the early 1950's in an endeavor to describe the cohesive properties of the so-called jellium—interacting electrons moving in a background of a uniform positive charge. Using a Hamiltonian formulation of interacting many-electron system, Bohm and Pines were able to decouple the collective motion of electrons—the plasma oscillations—from their individual motions, a procedure named as RPA. It was soon recognized [3] that the original RPA formulation is equivalent to the infinite summation of ring diagrams from the viewpoint of diagrammatic many-body perturbation theory [4]. Since then, the RPA concept has gone beyond the realm of condensed matter physics and significantly influenced all branches of physics.

Although the RPA concept can be applied to any interacting many-particle systems (for its applications in nuclear physics, see, e.g., Ref. [5]), in this review we shall restrict ourselves to electronic systems which are governed by Coulomb interactions. The next key step towards applying RPA to real materials was the incorporation of RPA into the Kohn-Sham (KS) density-functional theory (DFT) framework in 1970's [6–8]. This formulation turned RPA into a first-principles electronic-structure method, suitable for computing the ground-state energy of real materials. Within the KS-DFT framework, RPA can be viewed as a fifth-rung approximation to the exchange-correlation (XC) energy functional, according to a well-accepted classification scheme of the XC functionals, known as Jacob's ladder of DFT as proposed by Perdew [9]. However, the application of RPA to realistic systems was impeded by its high computational cost and the lack of efficient algorithms at the time. The first application of RPA to small molecules only appeared in early 2000's, carried out by Furche [10] and in [11]. Since then, RPA has been applied to a variety of systems including atoms [12,13], molecules [10,11,14–18], solids [19–26], surfaces [27,28], interfaces [29,30], layered materials [31], and defects [32,33]. The consensus arising from these studies is that RPA is capable of describing the delicate energy differences in complex chemical environments [27,28,24,26], the correct asymptotic behavior of van der Waals (vdW) complexes [34,35] and layered materials [31,36], and the correct dissociation limit of closed-shell molecules [10,11]. Evidence shows that RPA can provide unprecedented accuracy compared to lower-rung density-functional approximations at tractable computational cost. As such, RPA is expected to play an increasingly more important role in computational materials science, with the rapid development of more efficient algorithms and the availability of more powerful computing resources.

In a review paper [37] published in 2012, we discussed the history of the RPA concept, its formulation as a first-principles method, and its applications in quantum chemistry and computational materials science up to that time. These points were nicely summarized by David Pines in his recent review paper titled as "*Emergent behavior in strongly correlated electron systems*" [38]. In particular, Pines noted that,

> *Sixty-plus years later, the RPA continues to play a significant role in nuclear physics, bosonic field-theory, the quarkgluon plasma, many-fermion solvable models, and*

especially in computational chemistry and materials science. A recent review by Ren et al., to which the interested reader is referred, describes the impact of the RPA in the theoretical chemistry and materials science community, cites some thirty articles that indicate the renewed and widespread interest in the RPA during the period 2001-2011, discusses how it enables one to derive the $1/r^6$ interaction between spatially separated closed shell electron systems, and, shows, in some detail, how the RPA enables one to go beyond density-functional theory in computing ground state energies.

This highlights the far-reaching impact of the RPA in a variety of fields, in particular in computational chemistry and materials science. It is worthwhile to mention that several other, complementary RPA review papers also appeared around that time, where the theoretical foundation and applications of RPA are discussed from different perspective. More recent account of RPA of review character can be found in Ref. [39].

In this lecture, we first give an account of the theoretical foundation of RPA, highlighting its unique role in electronic structure theory. Computational schemes beyond RPA are also briefly discussed in this section. This is followed by a sketching of the key algorithm of implementing RPA using the resolution-of-identity technique. We then present some prototypical applications illustrating the usefulness of RPA in computational materials science. Most recent efforts devoted to further developing the theoretical and computational aspects of RPA as well as extending its capabilities are briefly mentioned and commented, before we conclude.

2 Theoretical foundation of RPA and beyond

RPA as a first-principles method can be derived from several theoretical frameworks. One convenient framework to derive RPA is the adiabatic-connection fluctuation-dissipation theorem (ACFDT) which offers a powerful mathematical device to construct the exact XC energy functional via the density response functions of a series of partially interacting systems, connecting the KS system and the true physical system. In this formulation, an approximation to the density response function translates into a corresponding approximation to the XC energy functional. However, this is not the only approach to formulate RPA. In fact, RPA can also be derived from other theoretical perspectives, including coupled cluster theory [40, 41], the Green-function based many-body perturbation theory [42, 37, 43], and time-dependent DFT [10]. Below we focus on the ACFDT perspective.

2.1 Adiabatic connection approach to DFT

An interacting N-electron system is described by the following Hamiltonian

$$\hat{H} = \hat{T} + \hat{V}_{\text{ext}} + \hat{V}_{\text{ee}} = -\sum_i^N \frac{\nabla_i^2}{2} + \sum_i^N v^{\text{ext}}(\hat{\mathbf{r}}_i) + \frac{1}{2} \sum_{i \neq j}^N \frac{1}{|\hat{\mathbf{r}}_i - \hat{\mathbf{r}}_j|} \,, \tag{1}$$

where $\hat{T}$, $\hat{V}_{\text{ext}}$, and $\hat{V}_{\text{ee}}$ are, respectively, the kinetic energy, the external potential, and the electron-electron Coulomb interaction operators. Hartree atomic units ($\hbar = e = m_e = 1$) are used throughout this lecture note. Note that the operators $\hat{T}$ and $\hat{V}_{\text{ee}}$ are universal for any N-electron systems, and a system is completely specified by the external potential,

$$v^{\text{ext}}(\mathbf{r}) = -\sum_\alpha \frac{Z_\alpha}{|\mathbf{R}_\alpha - \mathbf{r}|} , \tag{2}$$

with Z_α and $\mathbf{R}_\alpha$ being, respectively, the nuclear charges and positions of the atoms in the system. The Hamiltonian in (1) cannot be solved for more than a few electrons. To deal with it, it is customary to separate $\hat{H}$ into two parts,

$$\hat{H} = \hat{H}_0 + \hat{H}' \tag{3}$$

where $\hat{H}_0$ is a *mean-field* (MF) Hamiltonian, describing a collection of noninteracting particles subjecting to a self-consistently determined effective single-particle potential,

$$\hat{H}_0 = \sum_i^N \left(-\frac{\nabla_i^2}{2} + v^{\text{ext}}(\mathbf{r}_i) + v_i^{\text{MF}} \right) . \tag{4}$$

Here the mean-field potential v^{MF} is an average potential that one electron experiences due to the presence of other electrons. Different underlying principles to determine v^{MF} lead to different self-consistency schemes. Suppose Φ_0 is the ground-state wave function (a Slater determinant) of $\hat{H}_0$, within Hartree-Fock theory, the effective single-particle potential v^{MF} is chosen such that the expectation value of $\langle \Phi_0 | \hat{H} | \Phi_0 \rangle$ is minimized. On the other hand, within KS-DFT, the effective v^{MF} (now the KS potential v^{KS}) is determined so that the electron density of the KS system $n(\mathbf{r}) = \langle \Phi_0 | \hat{n}(\mathbf{r}) | \Phi_0 \rangle$ reproduces the density $n(\mathbf{r})$ of the true physical system. Within the adiabatic connection (AC) approach to KS-DFT, one considers a continuous set of fictitious Hamiltonians

$$\hat{H}(\lambda) = -\sum_i^N \frac{\nabla_i^2}{2} + \sum_i^N v_\lambda^{\text{aux}}(\hat{\mathbf{r}}_i) + \frac{\lambda}{2} \sum_{i \neq j}^N \frac{1}{|\hat{\mathbf{r}}_i - \hat{\mathbf{r}}_j|} , \tag{5}$$

which connects $\hat{H}_0$ at $\lambda = 0$ (with $v_{\lambda=0}^{\text{aux}} = v^{\text{ext}} + v^{\text{KS}}$) and $\hat{H}$ at $\lambda = 1$ (with $v_{\lambda=1}^{\text{aux}} = v^{\text{ext}}$). The Hamiltonian $\hat{H}(\lambda)$ for $0 < \lambda < 1$ describes a collection of particles moving under the auxiliary external potential $v_\lambda^{\text{aux}}(\mathbf{r})$ and interacting with a scaled Coulomb interaction $\lambda/|\mathbf{r} - \mathbf{r}'|$. The auxiliary potential $v_\lambda^{\text{aux}}(\mathbf{r})$ ($0 < \lambda < 1$) is chosen such that the density of λ-scaled systems is kept at the physical density, i.e., $n_\lambda(\mathbf{r}) = n(\mathbf{r})$, along the AC path. Denoting the ground-state wavefunction of $\hat{H}(\lambda)$ as $|\Psi_\lambda\rangle$,

$$\hat{H}(\lambda)|\Psi_\lambda\rangle = E_\lambda|\Psi_\lambda\rangle , \tag{6}$$

and adopting the normalization condition $\langle \Psi_\lambda | \Psi_\lambda \rangle = 1$, the Hellmann-Feynman theorem implies

that

$$
\begin{aligned}
\frac{dE_\lambda}{d\lambda} &= \left\langle \Psi_\lambda \middle| \frac{\partial \hat{H}_\lambda}{\partial \lambda} \middle| \Psi_\lambda \right\rangle = \left\langle \Psi_\lambda \middle| \sum_{i=1}^{N} \frac{\partial v_\lambda^{\mathrm{aux}}(\hat{\mathbf{r}}_i)}{\partial \lambda} + \frac{1}{2} \sum_{i\neq j}^{N} \frac{1}{|\hat{\mathbf{r}}_i - \hat{\mathbf{r}}_j|} \middle| \Psi_\lambda \right\rangle \\
&= \int d\mathbf{r} \left\langle \Psi_\lambda \middle| \hat{n}(\mathbf{r}) \frac{\partial v_\lambda^{\mathrm{aux}}(\mathbf{r})}{\partial \lambda} \middle| \Psi_\lambda \right\rangle + \frac{1}{2} \iint d\mathbf{r} d\mathbf{r}' \frac{\langle \Psi_\lambda | \hat{n}(\mathbf{r})\hat{n}(\mathbf{r}') - \hat{n}(\mathbf{r})\,\delta(\mathbf{r}-\mathbf{r}') | \Psi_\lambda \rangle}{|\mathbf{r}-\mathbf{r}'|} \quad (7) \\
&= \int d\mathbf{r}\, n(\mathbf{r}) \frac{\partial v_\lambda^{\mathrm{aux}}(\mathbf{r})}{\partial \lambda} + \frac{1}{2} \iint d\mathbf{r} d\mathbf{r}' \frac{\langle \Psi_\lambda | \hat{n}(\mathbf{r})\hat{n}(\mathbf{r}') | \Psi_\lambda \rangle - n(\mathbf{r})\delta(\mathbf{r}-\mathbf{r}')}{|\mathbf{r}-\mathbf{r}'|} \quad (8)
\end{aligned}
$$

To derive (7) and (8), we have used the expression for the density operator of the N-electron systems

$$
\hat{n}(\mathbf{r}) = \sum_{i=1}^{N} \delta(\mathbf{r} - \hat{\mathbf{r}}_i)\,, \tag{9}
$$

and the condition $\langle \Psi_\lambda | \hat{n}(\mathbf{r}) | \Psi_\lambda \rangle = n(\mathbf{r})$. The ground-state energy of the interacting system can then be obtained as

$$
\begin{aligned}
E &= E_0 + \int_0^1 \frac{dE_\lambda}{d\lambda}\, d\lambda \\
&= E_0 + \int d\mathbf{r}\, n(\mathbf{r}) \big(v_{\lambda=1}^{\mathrm{aux}}(\mathbf{r}) - v_{\lambda=0}^{\mathrm{aux}}(\mathbf{r}) \big) + \int_0^1 d\lambda\, \frac{1}{2} \iint d\mathbf{r} d\mathbf{r}' \frac{\langle \Psi_\lambda | \hat{n}(\mathbf{r})\hat{n}(\mathbf{r}') | \Psi_\lambda \rangle - n(\mathbf{r})\,\delta(\mathbf{r}-\mathbf{r}')}{|\mathbf{r}-\mathbf{r}'|} \\
&= E_0 - \int d\mathbf{r}\, n(\mathbf{r})\, v^{\mathrm{KS}}(\mathbf{r}) + \frac{1}{2} \iint d\mathbf{r}\, d\mathbf{r}' \frac{n(\mathbf{r})\, n(\mathbf{r}')}{|\mathbf{r}-\mathbf{r}'|} \\
&\quad + \int_0^1 d\lambda\, \frac{1}{2} \iint d\mathbf{r}\, d\mathbf{r}' \frac{\langle \Psi_\lambda | \delta\hat{n}(\mathbf{r})\delta\hat{n}(\mathbf{r}') | \Psi_\lambda \rangle - n(\mathbf{r})\delta(\mathbf{r}-\mathbf{r}')}{|\mathbf{r}-\mathbf{r}'|}\,, \quad (10)
\end{aligned}
$$

where we have introduced the fluctuation of the density operator $\delta\hat{n}(\mathbf{r}) = \hat{n}(\mathbf{r}) - n(\mathbf{r})$ and used the fact that $\langle \Psi_\lambda | \delta\hat{n}(\mathbf{r}) | \Psi_\lambda \rangle = 0$. Now the ground-state energy of the reference KS state ($\lambda = 0$) E_0 is given by

$$
E_0 = \langle \Psi_0 | \hat{H}_0 | \Psi_0 \rangle = \langle \Phi_0 | \hat{H}_0 | \Phi_0 \rangle = -\sum_{n=1}^{N} \left\langle \psi_n \middle| \frac{\nabla^2}{2} \middle| \psi_n \right\rangle + \int d\mathbf{r}\, v^{\mathrm{ext}}(\mathbf{r})\, n(\mathbf{r}) + \int d\mathbf{r}\, v^{\mathrm{KS}}(\mathbf{r})\, n(\mathbf{r})\,.
\tag{11}
$$

Combining (10) and (11), one arrives at the formal expression of the exact ground-state total energy of N-electron systems,

$$
\begin{aligned}
E &= -\sum_{n=1}^{N} \left\langle \psi_n \middle| \frac{\nabla^2}{2} \middle| \psi_n \right\rangle + \int d\mathbf{r}\, v^{\mathrm{ext}}(\mathbf{r})\, n(\mathbf{r}) + \frac{1}{2} \iint d\mathbf{r}\, d\mathbf{r}' \frac{n(\mathbf{r})n(\mathbf{r}')}{|\mathbf{r}-\mathbf{r}'|} \\
&\quad + \int_0^1 d\lambda\, \frac{1}{2} \iint d\mathbf{r}\, d\mathbf{r}' \frac{\langle \Psi_\lambda | \delta\hat{n}(\mathbf{r})\, \delta\hat{n}(\mathbf{r}') | \Psi_\lambda \rangle - n(\mathbf{r})\delta(\mathbf{r}-\mathbf{r}')}{|\mathbf{r}-\mathbf{r}'|}\,. \quad (12)
\end{aligned}
$$

In KS-DFT, the ground-state total energy for an interacting N-electron systems is an (implicit) functional of the electron density $n(\mathbf{r})$ and can be conveniently separated into four terms:

$$
E[n] = T_{\mathrm{s}}[\psi_n] + E_{\mathrm{ext}}[n] + E_{\mathrm{H}}[n] + E_{\mathrm{xc}}[n]\,, \tag{13}
$$

where

$$T_{\mathrm{s}} = -\sum_{n=1}^{N} \left\langle \psi_n \left| \frac{\nabla^2}{2} \right| \psi_n \right\rangle \tag{14}$$

is the kinetic energy of the KS independent-particle system,

$$E_{\mathrm{ext}}[n] = \int d\mathbf{r}\, v^{\mathrm{ext}}(\mathbf{r})\, n(\mathbf{r}) \tag{15}$$

is the external potential energy due to the nuclei,

$$E_{\mathrm{H}}[n] = \frac{1}{2} \iint d\mathbf{r}\, d\mathbf{r}' \frac{n(\mathbf{r})n(\mathbf{r}')}{|\mathbf{r}-\mathbf{r}'|} \tag{16}$$

is the classic Hartree energy, and E_{xc} the exchange-correlation energy. Among the four terms in Eq. (13), only $E_{\mathrm{ext}}[n]$ and $E_{\mathrm{H}}[n]$ are explicit functionals of $n(\mathbf{r})$. The noninteracting kinetic energy T_{s} is treated exactly in KS-DFT in terms of the single-particle KS orbitals $\psi_n(\mathbf{r})$, which themselves are a functional of $n(\mathbf{r})$. All the many-body complexity is contained in the unknown XC energy term, whose exact form is not an explicit functional of the electron density $n(\mathbf{r})$, nor the KS orbitals $\psi_n(\mathbf{r})$. Comparing Eq. (13) to (12), one immediately obtains the formally exact AC expression for the XC energy, in terms of the density-density correlation function,

$$E_{\mathrm{xc}}[n] = \int_0^1 d\lambda \frac{1}{2} \iint d\mathbf{r}\, d\mathbf{r}' \frac{\langle \Psi_\lambda | \delta\hat{n}(\mathbf{r})\, \delta\hat{n}(\mathbf{r}') | \Psi_\lambda \rangle - n(\mathbf{r})\delta(\mathbf{r}-\mathbf{r}')}{|\mathbf{r}-\mathbf{r}'|} \,. \tag{17}$$

A central task of the DFT community is to develop accurate and tractable approximations to $E_{\mathrm{xc}}[n]$. The success of KS-DFT lies in the fact that usefully accurate approximations can be found, for which DFT calculations can be done at affordable cost. Widely used approximations to $E_{\mathrm{xc}}[n]$ include local-density approximation (LDA) [44], generalized gradient approximations (GGAs) [45–47], meta-GGA [48,49], and hybrid functional approximations [50,51]. These approximations belong to the first four rungs of the Jacob's ladder [9]. Despite their enormous success, these existing approximate functionals suffer from many-electron self-interaction errors [52], or delocalization errors [53] due to which the localized electronic states tend to delocalize over the system, leading to several severe consequences. Furthermore, the non-local correlation effects between widely separated subsystems are not captured within these approximations by constructions. These intrinsic deficiencies limit the possible accuracy that can be achieved in practical calculations. Qualitative and sometimes quantitative failures have been documented in a number of situations, among which the most prominent are van der Waals (vdW) bonded systems [54], materials with strong correlations [55], certain surface adsorption problems [56], and chemical reaction barrier heights [57].

2.2 RPA derived from the ACFDT framework

The construction of LDA, GGA, and meta-GGA functionals only incorporate local and semi-local quantities, such as the electron density, density gradients, and the kinetic energy density. For the construction of hybrid functionals, a non-local quantity—the reduced density matrix—is

required. To go beyond these approximations, it is necessary to include additional information in the functional construction. For this purpose, it is instrumental to invoke the zero-temperature fluctuation-dissipation theorem [58], which relates the density-density correlation (*fluctuations*) in Eq. (17) to the imaginary part of the density response function (*dissipation*) of the system

$$\langle \Psi_\lambda | \delta \hat{n}(\mathbf{r})\, \delta \hat{n}(\mathbf{r}') | \Psi_\lambda \rangle = -\frac{1}{2\pi} \int_{-\infty}^{\infty} d\omega \, \mathrm{Im}\, \chi^\lambda(\mathbf{r}, \mathbf{r}', \omega) \,. \tag{18}$$

Here the density response function $\chi^\lambda(\mathbf{r}, \mathbf{r}', \omega) = \delta n_\lambda(\mathbf{r}, \omega)/\delta v^{ext}(\mathbf{r}', \omega)$ describes the variation of the density of the partially interacting system at the spatial point $\mathbf{r}$, up to linear order, due to a change of the local external potential at $\mathbf{r}'$. From Eqs. (17) and (18), we arrive at the renowned ACFDT expression for the XC energy in DFT

$$E_{\mathrm{xc}} = \frac{1}{2} \int_0^1 d\lambda \iint d\mathbf{r}\, d\mathbf{r}' \frac{1}{|\mathbf{r}-\mathbf{r}'|} \left(-\frac{1}{2\pi} \int_{-\infty}^{\infty} d\omega \, \mathrm{Im}\, \chi^\lambda(\mathbf{r}, \mathbf{r}', \omega) - \delta(\mathbf{r}-\mathbf{r}')\, n(\mathbf{r}) \right)$$

$$= \frac{1}{2} \int_0^1 d\lambda \iint d\mathbf{r}\, d\mathbf{r}' \frac{1}{|\mathbf{r}-\mathbf{r}'|} \left(-\frac{1}{\pi} \int_0^{\infty} d\omega \; \chi^\lambda(\mathbf{r}, \mathbf{r}', i\omega) \; - \; \delta(\mathbf{r}-\mathbf{r}')\, n(\mathbf{r}) \right) \,. \tag{19}$$

The fact that the above frequency integration can be performed along the imaginary axis originates from the analytical structure of $\chi^\lambda(\mathbf{r}, \mathbf{r}', \omega)$ and the fact that it becomes purely real on the imaginary axis. Such a property simplifies the ground-state energy calculation within the ACFDT framework considerably. The ACFDT expression in Eq. (19) transforms the problem of computing the XC energy to the computation of the response functions of a continuous set of fictitious systems along the AC path, which in practice has to be approximated as well.

The exact density response function $\chi^\lambda(\mathbf{r}, \mathbf{r}', i\omega)$ is not known either. However, according to linear-response time-dependent DFT (TDDFT), the interacting response function χ^λ for $\lambda > 0$ is linked to the noninteracting response function χ^0 via the Dyson-like equation

$$\chi^\lambda(\mathbf{r}, \mathbf{r}', i\omega) = \chi^0(\mathbf{r}, \mathbf{r}', i\omega) + \int d\mathbf{r}_1\, d\mathbf{r}_2\, \chi^0(\mathbf{r}, \mathbf{r}_1, i\omega) \left[\frac{\lambda}{|\mathbf{r}_1-\mathbf{r}_2|} + f_{\mathrm{xc}}^\lambda(\mathbf{r}_1, \mathbf{r}_2, i\omega) \right] \chi^\lambda(\mathbf{r}_2, \mathbf{r}', \omega) \,, \tag{20}$$

where

$$f_{xc}(\mathbf{r}_1, \mathbf{r}_2, i\omega) = \frac{\delta v_{\mathrm{xc}}(\mathbf{r}_1)}{\delta n(\mathbf{r}_2, \omega)} = \frac{\delta^2 E_{\mathrm{xc}}[n]}{\delta n(\mathbf{r}_1) \delta n(\mathbf{r}_2, \omega)} \tag{21}$$

is the so-called f_{xc} kernel, given by the functional derivative of the XC potential with respect to the frequency-dependent density variation.

Obviously, the f_{xc} kernel is a very complex quantity to deal with, and there are considerable ongoing efforts to find better approximations for it [59]. In this context, the *random phase approximation* amounts to simply neglecting the f_{xc} kernel, and the resultant interacting response function is termed the RPA response function,

$$\chi_{\mathrm{RPA}}^\lambda(\mathbf{r}, \mathbf{r}', i\omega) = \chi^0(\mathbf{r}, \mathbf{r}', i\omega) + \int d\mathbf{r}_1\, d\mathbf{r}_2\, \chi^0(\mathbf{r}, \mathbf{r}_1, i\omega) \frac{\lambda}{|\mathbf{r}-\mathbf{r}'|} \chi_{\mathrm{RPA}}^\lambda(\mathbf{r}_2, \mathbf{r}', \omega) \,. \tag{22}$$

In physical terms, the RPA here corresponds to the linearized time-dependent Hartree approximation, by which the variation of the exchange-correlation potential due to an external perturbation is neglected.

In Eqs. (20) and (22), $\chi^0(\mathbf{r}, \mathbf{r}_1, i\omega)$ is the independent-particle response function of the KS reference system ($\lambda = 0$) and is known explicitly in terms of the single-particle KS orbitals $\psi_n(\mathbf{r})$, orbital energies ε_n, and occupation factors f_n

$$\chi^0(\mathbf{r}, \mathbf{r}', i\omega) = \sum_{mn} \frac{(f_m - f_n)\psi_m^*(\mathbf{r})\psi_n(\mathbf{r})\psi_n^*(\mathbf{r}')\psi_m(\mathbf{r}')}{\varepsilon_m - \varepsilon_n - i\omega} . \tag{23}$$

Based on Eqs. (19) and (22), the XC energy in RPA can be further decomposed into an exact exchange (EX) term and a RPA correlation term,

$$E_{xc}^{RPA} = E_x^{EX} + E_c^{RPA}, \tag{24}$$

where

$$\begin{aligned} E_x^{EX} &= \frac{1}{2} \iint d\mathbf{r}\, d\mathbf{r}' \frac{1}{|\mathbf{r}-\mathbf{r}'|} \left(-\frac{1}{\pi} \int_0^\infty d\omega\, \chi^0(\mathbf{r}, \mathbf{r}', i\omega) - \delta(\mathbf{r}-\mathbf{r}')n(\mathbf{r}) \right) \\ &= -\sum_{mn} f_m f_n \iint d\mathbf{r}\, d\mathbf{r}' \frac{\psi_m^*(\mathbf{r})\psi_n(\mathbf{r})\psi_m^*(\mathbf{r}')\psi_n(\mathbf{r}')}{|\mathbf{r}-\mathbf{r}'|} \end{aligned} \tag{25}$$

and

$$\begin{aligned} E_c^{RPA} &= -\frac{1}{2\pi} \iint d\mathbf{r}\, d\mathbf{r}' \frac{1}{|\mathbf{r}-\mathbf{r}'|} \int_0^\infty d\omega \left(\int_0^1 d\lambda\, \chi_{RPA}^\lambda(\mathbf{r}, \mathbf{r}', i\omega) - \chi_0(\mathbf{r}, \mathbf{r}', i\omega) \right) \\ &= \frac{1}{2\pi} \int_0^\infty d\omega\, \mathrm{Tr}\left(\ln\left(1 - \chi^0(i\omega)v\right) + \chi^0(i\omega)\, v \right), \end{aligned} \tag{26}$$

with $v(\mathbf{r}, \mathbf{r}') = 1/|\mathbf{r}-\mathbf{r}'|$. Equation (25) defines the exact-exchange energy in the KS-DFT context, which has the same expression as the Hartree-Fock exchange energy, but is extended here to fractional occupation numbers and to be evaluated with KS orbitals. Furthermore, in the second line of Eq. (26), for brevity the following convention

$$\mathrm{Tr}\,[fg] = \iint d\mathbf{r}\, d\mathbf{r}'\, f(\mathbf{r}, \mathbf{r}')\, g(\mathbf{r}', \mathbf{r}) \tag{27}$$

has been adopted.

So far, we have described how the RPA method is defined as an approximate XC energy functional in the KS-DFT context, within the ACFDT framework. As mentioned above, RPA can also be derived from the perspective of coupled cluster theory and the Green-function based many-body perturbation theory. For instance, from the perspective of the ring coupled cluster doubles (rCCD) theory, the RPA correlation energy can be obtained as,

$$E_c^{RPA} = \frac{1}{2}\mathrm{Tr}\left(BT^{rCCD}\right) = \frac{1}{2} \sum_{ij,ab} B_{ia,jb}T_{jb,ia}^{rCCD}, \tag{28}$$

where $T_{jb,ia}^{rCCD}$ is the rCCD amplitude, to be determined by solving the so-called Riccati equation [41], and $B_{ia,jb} = \langle ij|ab \rangle$ with $\langle ij|ab \rangle$ being two-electron Coulomb integrals,

$$\langle ij|ab \rangle = \iint d\mathbf{r}\, d\mathbf{r}' \frac{\psi_i^*(\mathbf{r})\psi_a(\mathbf{r})\psi_j^*(\mathbf{r}')\psi_b(\mathbf{r}')}{|\mathbf{r}-\mathbf{r}'|} . \tag{29}$$

Here and below, we adopt the convention that i, j, k refer to occupied KS orbitals, a, b, c to virtual (unoccupied) orbitals, and m, n to general ones. Due to limited space, here we will not elaborate on the alternative formulations of RPA any further, and interested readers are referred to Ref. [37] and the original references [41, 42] for more details.

2.3   Beyond-RPA computational schemes

Despite its appealing features, RPA does not go without shortcomings. The conventional wisdom is that RPA describes the long-range correlation very well, whereas it is not adequate for short-range correlations. This issue has been well known for the homogeneous electron gas. For real materials, RPA was found to underestimate the cohesive energies of both molecules [10,60] and solids [21]. This stimulated much research interest and several beyond-RPA schemes have been developed to fix this deficiency. Among these, two approaches are particularly noteworthy: 1) improving RPA by restoring the contribution of the f_{xc} kernel within the ACFDT formalism; 2) improving RPA from the perspective of diagrammatic many-body perturbation theory. Successful beyond-RPA schemes of the first type include the truncated adiabatic LDA kernel correction [61], and the more systematic construction of the XC kernel with respect to a series expansion of the coupling constant λ within the ACFDT framework [62,59].

The diagrammatic many-body expansion approach to correct RPA, on which we shall concentrate here, exploits the fact that RPA, in contrast with other density-functional approximations (DFAs), has a clear diagrammatic representation—an infinite summation of the ring diagrams. The question arises if there is a simple and systematic way to incorporate the missing diagrams to arrive at an improved theory. The fermionic nature of electrons requires the many-electron wavefunction to be antisymmetric, and the diagrammatic representation of the correlation energy contains graphs describing both *direct* processes and *exchange* processes. For example, in the Møller-Plesset perturbation theory, both types of processes are included at each order, which ensures the theory to be one-electron "self-correlation free"—the correlation energy for one-electron system being zero. The famous second-order Møller-Plesset perturbation theory (MP2), a widely used method in quantum chemistry, contains one *direct* term and one *exchange* term, represented respectively by the leading diagram in the first two rows of Fig. 1. These two terms cancel each other for one-electron systems. RPA is represented by the ring diagrams summed up to infinite order, as represented by the first-row diagrams in Fig. 1, where only "direct" processes are accounted for.[1] A simple way to include the exchange processes and eliminate the self-correlation error is to *antisymmetrize* the two-electron Coulomb integrals within the rCCD formulation of RPA [cf. Eq. (28)]. By doing so, a second-order screened exchange (SOSEX) term [63–65] is added, and the resultant RPA+SOSEX correlation energy is given by

$$E_c^{\text{RPA+SOSEX}} = \frac{1}{2} \sum_{ij,ab} \left(\langle ij|ab \rangle - \langle ij|ba \rangle \right) T_{ia,jb}^{\text{rCCD}} \, , \tag{30}$$

---

[1]The RPA discussed here is often referred to as *direct* RPA in quantum chemistry literature. In some literature, RPA in fact corresponds to the time-dependent Hartree-Fock theory, where the exchange terms are also included. Nowadays, RPA with exchange included is usually referred to as RPAX or *full* RPA.
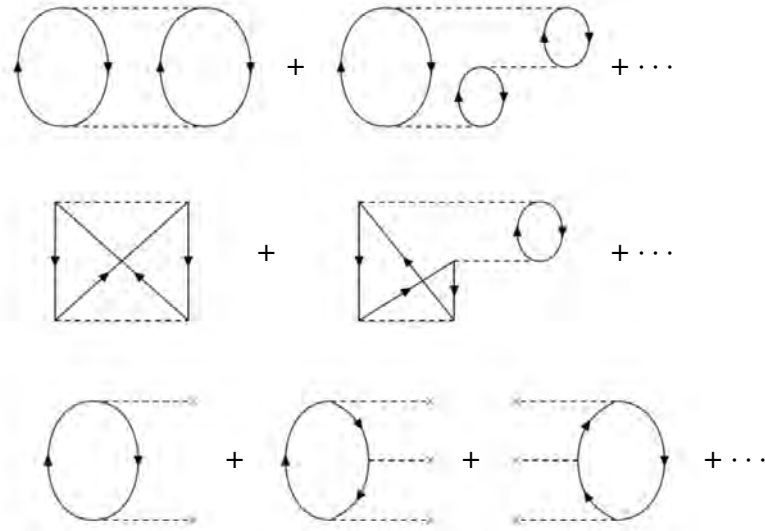
Fig. 1: *Goldstone diagrams for rPT2. Diagrams in the three rows correspond to RPA, SOSEX, and rSE, respectively. Dashed lines ending with a cross in the third row denote the matrix element $\Delta v_{mn} = \langle \psi_m | \hat{v}^{HF} - \hat{v}^{MF} | \psi_n \rangle$. The rules to evaluate Goldstone diagrams can be found in Ref. [66].*

with the two terms in Eq. (30) corresponding to RPA and SOSEX correlation energies respectively. The SOSEX contribution can be represented by the diagrams shown in the second row of Fig. 1, where the leading term corresponds to the exchange contribution in MP2. The RPA+SOSEX scheme has the interesting feature that it is one-electron self-correlation free, and improves substantially the total energy [64, 65]. The underbinding problem of RPA for chemically bonded molecules and solids is on average alleviated by the SOSEX correction.

As illustrated in Fig. 1, both RPA and SOSEX correlations can be interpreted as *infinite-order summations of selected types of diagrams*, with the MP2 terms as the leading order. This perspective is helpful for identifying important contributions that are still missing in the RPA+SOSEX scheme. In fact, at the second-order, in addition to the direct and exchange terms, there is yet another type of contribution, arising from the singles excitations (SE),

$$
E_c^{SE} = \sum_i^{occ} \sum_a^{unocc} \frac{|\langle \Phi_0 | \hat{H}' | \Phi_i^a \rangle|^2}{E_0 - E_{i,a}^{(0)}} = \sum_{ia} \frac{|\langle \psi_i | \hat{v}^{HF} - \hat{v}^{MF} | \psi_a \rangle|^2}{\varepsilon_i - \varepsilon_a} = \sum_{ia} \frac{\left|\langle \psi_i | \hat{f} | \psi_a \rangle\right|^2}{\varepsilon_i - \varepsilon_a} , \qquad (31)
$$

where $\hat{v}^{HF}$ is the self-consistent Hartree-Fock potential, $\hat{v}^{MF}$ is the mean-field potential, based on which the reference state is generated, and $\hat{f} = -\nabla^2/2 + \hat{v}^{ext} + \hat{v}^{HF}$ is the single-particle Hartree-Fock Hamiltonian (also known as the Fock matrix in the quantum chemistry literature). Φ_0 and Φ_i^a are the KS Slater determinant and the singly-excited configuration generated by exciting one electron from an occupied state i to a virtual state a. A detailed derivation of Eq. (31) can be found in the supplementary material of Ref. [17]. Obviously for a Hartree-Fock reference where $\hat{v}^{MF} = \hat{v}^{HF}$, Eq. (31) becomes zero, a fact known as Brillouin theorem [66]. Therefore, this term is not present in standard MP2 theory based on the Hartree-Fock reference.

In Ref [17], it was shown that adding the SE term of Eq. (31) to RPA significantly improves the accuracy of vdW-bonded molecules, which the standard RPA scheme generally underbinds, and the SOSEX correction does not improve much. Similar to the RPA and SOSEX case, one can identify a sequence of single-excitation processes up to infinite order, as illustrated in the third row in Fig. 1. Summing these single-excitation diagrams up to infinite order represents a renormalization of the 2nd-order SE, and is termed as renormalized singles excitations (rSE) [37,35]. Remarkably, this infinite summation ends up with a closed expression similar to Eq. (31) ,

$$E_c^{\mathrm{rSE}} = \sum_{ia} \frac{|\tilde{f}_{ia}|^2}{\tilde{\varepsilon}_i - \tilde{\varepsilon}_a} \,, \tag{32}$$

where $\tilde{\varepsilon}_i$ and $\tilde{\varepsilon}_a$ are the eigenvalues obtained by diagonalizing separately the occupied-occupied and virtual-virtual subblocks of the Fock matrix,

$$\begin{aligned} \sum_k f_{ik}\, \mathcal{O}_{kj} &= \tilde{\varepsilon}_i\, \mathcal{O}_{ij} \\ \sum_c f_{ac}\, \mathcal{U}_{cb} &= \tilde{\varepsilon}_a\, \mathcal{U}_{ab} \,, \end{aligned} \tag{33}$$

with $f_{mn} = \langle \psi_m | \hat{f} | \psi_n \rangle$. Note that the matrix f_{mn} is not diagonal since the ψ_n are the reference KS orbitals and hence not the eigenfunctions of $\hat{f}$, which is the single-particle Hartree-Fock Hamiltonian. Now $\tilde{f}_{ia}$ in the numerator of Eq. (32) are to the "transformed" off-diagonal block of the Fock matrix

$$\tilde{f}_{ia} = \sum_{jb} \mathcal{O}^*_{ij}\, f_{jb}\, \mathcal{U}_{ba} \,, \tag{34}$$

where the eigenvectors obtained in (33) are used here as the transformation coefficients. The physical origin of the SE corrections is that the commonly used KS references for RPA and beyond-RPA calculations are not the optimal starting point. The SE corrections accounts for the "orbital relaxation" effect, which leads to a lowering of the ground-state total energy.

Diagrammatically, RPA, SOSEX and rSE are three distinct infinite series of many-body terms, in which the three leading terms correspond to the three terms in second-order many-body perturbation theory. Summing them up, the resultant RPA+SOSEX+rSE scheme can be viewed a *renormalization* of the normal second-order many-body perturbation theory. Therefore the RPA+SOSEX+rSE scheme is also termed as "*renormalized second-order perturbation theory*" or rPT2 in the literature.

Independent of the rPT2 scheme described above, Bates, and Furche developed a beyond-RPA formalism termed as RPA renormalized many-body perturbation theory [67]. The essence of this formalism is to express the correlation energy in terms of an integration over the polarization propagator (closely related to the density response function) along the AC path. The correlation energy can be improved by improving the polarization propagator based on a series expansion in terms of the RPA polarization propagator multiplied with a four-point kernel. Benchmark calculations [68] show that the approximate exchange kernel (AXK) scheme within this formalism performs better than RPA+SOSEX discussed above. However, the rSE contribution is not included in the AXK scheme.

3   Implementation of the RPA method

In most practical RPA calculations, the evaluation of the RPA XC energy $E_{\mathrm{xc}}^{\mathrm{RPA}}$ as given in Eqs. (24-26) is done employing the KS orbitals and orbital energies generated by a preceding KS-DFT calculation under certain lower-rung approximations. The GGA of Perdew, Burke, and Ernzerhof (PBE) is often used in the preceding KS-DFT calculation, and the RPA calculation based on a PBE reference is often denoted as "RPA@PBE." In standard RPA@PBE calculations, the ground-state total energy is given by

$$
\begin{aligned}
E^{\mathrm{RPA@PBE}} &= E^{\mathrm{PBE}} - E_{\mathrm{xc}}^{\mathrm{PBE}} + E_{\mathrm{xc}}^{\mathrm{RPA@PBE}} \\
&= T_s^{\mathrm{PBE}} + E_{\mathrm{ext}}^{\mathrm{PBE}} + E_{\mathrm{H}}^{\mathrm{PBE}} + E_{\mathrm{x}}^{\mathrm{EX@PBE}} + E_{\mathrm{c}}^{\mathrm{RPA@PBE}} \\
&= \langle \Phi_{\mathrm{PBE}} | \hat{H} | \Phi_{\mathrm{PBE}} \rangle + E_{\mathrm{c}}^{\mathrm{RPA@PBE}}
\end{aligned}
\tag{35}
$$

where T_s^{PBE}, $E_{\mathrm{ext}}^{\mathrm{PBE}}$, $E_{\mathrm{H}}^{\mathrm{PBE}}$, and $E_{\mathrm{xc}}^{\mathrm{PBE}}$ are, respectively, the noninteracting kinetic energy, the external potential energy, the Hartree energy, and the XC energy obtained from the self-consistent PBE calculation. The RPA@PBE total energy defined in (35) is obtained by subtracting the PBE XC energy from the PBE total energy, and then adding on top the RPA XC energy, evaluated using PBE orbitals and orbital energies. Equation (35) indicates that the RPA total energy can be seen as the sum of the Hartree-Fock energy evaluated with respect to the PBE reference and the RPA@PBE correlation energy.

Now it is clear that the key in RPA calculations is to evaluate the exact-exchange energy plus the RPA correlation energy. The algorithm for evaluating the exact-exchange energy in the present context is exactly the same as the Hartree-Fock exchange energy evaluation, which is routinely done in quantum chemistry calculations [69,70]. The Hartree-Fock exchange is also a key component of hybrid density-functionals, which are available in increasingly more software that can deal with periodic systems [71,72]. Here we shall not discuss the implementation of the Hartree-Fock exchange, but rather focus on the implementation of the RPA correlation energy part. To develop efficient algorithms to evaluate Eq. (26), the key is to realize that both χ^0 and v are non-local operators in space. Their real-space forms $\chi^0(\mathbf{r}, \mathbf{r}', i\omega)$ and $v(\mathbf{r}, \mathbf{r}')$ can be seen as basis representations of the corresponding operator χ^0 and v in terms of real-space grid points. Under such a discretization, χ^0 and v become matrices of dimension as large as the number of real space grid points. This is not an efficient representation since the number of grid points is rather large, especially in all-electron calculations. To deal with this problem, one can introduce an auxiliary basis set $\{P_\mu(\mathbf{r})\}$ to represent χ^0 and v, namely,

$$
\chi^0(\mathbf{r}, \mathbf{r}', i\omega) = \sum_{\mu,\nu}^{N_{\mathrm{aux}}} P_\mu(\mathbf{r})\, \chi_{\mu\nu}^0(i\omega)\, P_\nu(\mathbf{r}'),
\tag{36}
$$

and

$$
V_{\mu\nu} = \iint d\mathbf{r}\, d\mathbf{r}'\, \frac{P_\mu(\mathbf{r}) P_\nu(\mathbf{r}')}{|\mathbf{r}-\mathbf{r}'|}
\tag{37}
$$

where N_{aux} is the number of auxiliary basis functions. To find the matrix form $\chi_{\mu,\nu}^0(i\omega)$, one

needs to expand the products of KS orbitals in terms of $P_\mu(\mathbf{r})$,

$$\psi_m^*(\mathbf{r})\psi_n(\mathbf{r}) = \sum_\mu C_{mn}^\mu P_\mu(\mathbf{r})\,, \tag{38}$$

where C_{mn}^μ is the expansion coefficients. Inserting the expansion (38) into (23), and comparing to (36), one arrives at

$$\chi_{\mu\nu}^0(i\omega) = \sum_{m,n} \frac{(f_m - f_n)\,C_{mn}^\mu\,C_{mn}^{\nu*}}{\varepsilon_m - \varepsilon_n - i\omega}\,. \tag{39}$$

Thus, within the auxiliary basis representation, χ^0 and v become $N_{\text{aux}} \times N_{\text{aux}}$ matrices. Since N_{aux} is typically much smaller than the number of real-space grid points, or the number of pair products of KS orbitals, the χ^0 matrix in (39) and the V matrix in (38) can be seen as compressed representation of their operators, with the trace of their product unchanged,

$$\text{Tr}\,\chi^0(i\omega)\,v = \iint \chi^0(\mathbf{r},\mathbf{r}',i\omega)\,v(\mathbf{r}',\mathbf{r})\,d\mathbf{r}\,d\mathbf{r}' = \sum_{\mu\nu} \chi_{\mu\nu}^0(i\omega)\,V_{\mu\nu}\,. \tag{40}$$

Based on this observation, one may conclude that the computed RPA correlation energy is independent of the basis representation of the χ^0 and v operators. Thus one may equivalently interpret Eq. (26) as matrix algebra with χ^0 and v represented within the auxiliary basis as given by (39) and (37). Using $\text{Tr}\,\ln A = \ln\det A$ (with $\det A$ being the determinant of the matrix A), one obtains the final working expression for evaluating the RPA correlation energy,

$$\begin{aligned}
E_{\text{c}}^{\text{RPA}} &= \frac{1}{2\pi} \int_0^\infty d\omega\, \ln\left(\det(1-\chi^0(i\omega)\,v) + \chi^0(i\omega)\,v\right)\\[2mm]
&= \frac{1}{2\pi} \int_0^\infty d\omega\, \ln\left(\det(1-\Pi(i\omega)) + \Pi(i\omega)\right)\,.
\end{aligned} \tag{41}$$

In Eq. (41), we have introduced an intermediate quantity $\Pi(i\omega) = V^{1/2}\,\chi^0(i\omega)\,V^{1/2}$ and used the property $\text{Tr}(V^{1/2}\,\chi^0\,V^{1/2}) = \text{Tr}(\chi^0\,V)$. The frequency integration in Eq. (41) can be done relatively easily, since the integrand is rather smooth and peaked at low frequency values. A modified Gauss-Legendre grid, which transforms a standard Gauss-Legendre grid in the range $[-1,1]$ to $[0,\infty]$,

$$\tilde{x}_i = x_0\,\frac{1+x_i}{1-x_i}\,, \qquad \tilde{w}_i = w_i\,\frac{2x_0}{(1-x_i)^2} \tag{42}$$

works rather well for most systems. In (42), (x_i, w_i) are the abscissas and weights of the grid points generated from the Gauss-Legendre quadrature formula in an integration range $[-1,1]$, whereas $(\tilde{x}_i, \tilde{w}_i)$ are abscissas and weights of the transformed grid. Usually a few tens of frequency grid points are sufficient to get highly accurate results, except for systems with vanishing gaps, where considerably more grid points have to be used. Alternative frequency grids have been developed for evaluating the RPA correlation energies [73, 33], which have been shown to work well for small gap systems.

The implementation scheme described above is known as the resolution-of-identity (RI) approach to RPA [73, 74]. From the above discussion, one may see that once the matrix forms of χ^0 and v within the auxiliary basis are determined, the rest of the RPA calculation is rather straightforward. The key steps in RPA calculations are thus: 1) Generate the auxiliary basis functions $\{P_\mu(\mathbf{r})\}$; 2) Determine the triple coefficients $C_{m,n}^\mu$; and 3) Construct the $\chi_{\mu,\nu}^0$ matrix using (39). The choice of auxiliary basis functions $\{P_\mu(\mathbf{r})\}$ depends on the underlying one-electron basis functions used in the KS-DFT calculations. Our own RPA implementation was done in the FHI-aims code [75, 74] which employs atom-centered numeric orbitals (NAOs) as basis functions

$$\phi_i(\mathbf{r}) = u_k(r)Y_{lm}(\theta, \phi) \,, \tag{43}$$

where $u_k(r)$ is a numerically tabulated radial function and $Y_{lm}(\theta, \phi)$ is a spherical harmonic. Our auxiliary basis functions are also constructed as a numerical radial function multiplied by spherical harmonics

$$P_\mu(\mathbf{r}) = \xi_s(r)Y_{lm}(\theta, \phi) \tag{44}$$

but the radial function $\xi_s(r)$ has a different shape from $u_k(r)$. In fact, they are generated in order to best represent the product of the one-electron orbitals $\phi_i\phi_j$. Details on how the auxiliary basis functions are constructed can be found in Refs. [74, 76].

Once the auxiliary basis functions $\{P_\mu(\mathbf{r})\}$ are constructed, we can start to determine the triple expansion coefficients $C_{m,n}^\mu$. For any finite auxiliary basis set, the expansion in (38) is an approximation, incurring an error $\delta\rho_{mn}(\mathbf{r}) = \sum_\mu C_{mn}^\mu P_\mu(\mathbf{r}) - \psi_m^*(\mathbf{r})\psi_n(\mathbf{r})$. The accuracy of this approximation will not only depend on the quality and size of the auxiliary basis, but also on the expansion coefficients $C_{m,n}^\mu$. In the RI approach with Coulomb metric [77], instead of minimizing the norm of the error $(\delta\rho_{mn}|\delta\rho_{mn})$, one minimizes the self Coulomb repulsion of this error $(\delta\rho_{mn}|v|\delta\rho_{mn})$, leading to the following expression for $C_{m,n}^\mu$,

$$C_{m,n}^\mu = \sum_\nu (mn|v|\nu) \, V_{\nu\mu}^{-1} \,, \tag{45}$$

where

$$(mn|v|\nu) = \iint d\mathbf{r} \, d\mathbf{r}' \, \frac{\psi_m^*(\mathbf{r})\psi_n(\mathbf{r})P_\nu(\mathbf{r}')}{|\mathbf{r}-\mathbf{r}'|} \,, \tag{46}$$

and V^{-1} is the inverted Coulomb matrix. This conventional (global) RI approach works extremely well for small molecules. For big molecules and periodic systems, one may switch to a localized variant of the RI approach [76]. With enhanced auxiliary basis functions, the localized RI approach has been shown to be sufficiently accurate in practical calculations [76], and is instrumental for periodic systems [72].

A final key step is to build the χ^0 matrix in (39). Since the number of auxiliary basis functions N_{aux} scales linearly with the number of one-electron basis functions, the computational cost of Eq. (39) scales as $O(N^4)$ with respect to the size of the system, and represents the computational bottleneck of RPA calculations. In recent years, lower-scaling algorithms have also been developed [33, 78], which holds promise for extending the applicability of RPA to large systems.

4   The performance of RPA-based methods and prototypical applications

The revived interest in RPA in recent years comes not only from its appealing concept, but also from its remarkable performance in practical applications. First of all, RPA can describe vdW interactions in a seamless way. The reason behind this capability has already been clearly explained by Dobson in the early days [79], and the performance of RPA has been demonstrated later for rare-gas crystals [19] and rare-gas dimers [17]. For lower-rung density-functional approximations (DFAs) ranging from LDA to hybrid functionals, the long-range vdW interactions are not captured, and *ad hoc* corrections have to be added in order to describe systems where vdW interactions play an important role. Furthermore, it seems that RPA is able to describe the delicate energy differences in complex bonding situations, including molecules adsorbed on surfaces [27, 28], the isostructural phase transition [24] and the relative stability of different polymorphs of crystals [26], the binding and ex-foliation energies of layered compounds [36], and the formation energy of defects [33]. Finally, RPA yields accurate chemical reaction barrier heights [37], which is crucial for reliably estimating the rate of chemical reactions.

4.1   Van der Waals interactions

Van der Waals (vdW) interactions arise from the coupling between spontaneous quantum charge fluctuations separated in space. For two well-separated, spherically-symmetric charge-neutral systems, the interaction energy goes like

$$\Delta E \sim \frac{C_6}{R^6} \quad \text{for } R \to \infty \tag{47}$$

where C_6 is the dispersion coefficient and R is the separation between the two systems. Dobson showed that the interaction energy between two subsystems A and B obtained by RPA exactly follows the asymptotic behavior given by (47), with the RPA C_6 coefficients given by

$$C_6^{\text{RPA}} = \frac{3}{\pi} \int d\omega \, \alpha_A^{\text{RPA}}(i\omega) \, \alpha_B^{\text{RPA}}(i\omega) \tag{48}$$

where $\alpha_A^{\text{RPA}}(i\omega)$ is the RPA polarizability of the subsystem A, which can be obtained by integrating over the microscopic RPA response function as,

$$\alpha_A^{\text{RPA}}(i\omega) = \frac{1}{3} \sum_{i=1}^{3} \iint d\mathbf{r} \, d\mathbf{r}' \, r_i \, \chi^{\text{RPA}}(\mathbf{r}, \mathbf{r}', i\omega) \, r_i' \tag{49}$$

with $r_{1,2,3} = x, y, z$.

In Fig. 2, the binding energy curves of Ar_2 obtained using PBE and RPA-based methods are presented. MP2 is the simplest post-Hartree-Fock quantum chemistry approach capable of describing vdW interactions, and hence also included here for comparison. The reference curve is given by the Tang-Toennies potential model, with model parameters determined from experiment. PBE underestimates the bonding strength of Ar_2 considerably, and this is appreciably
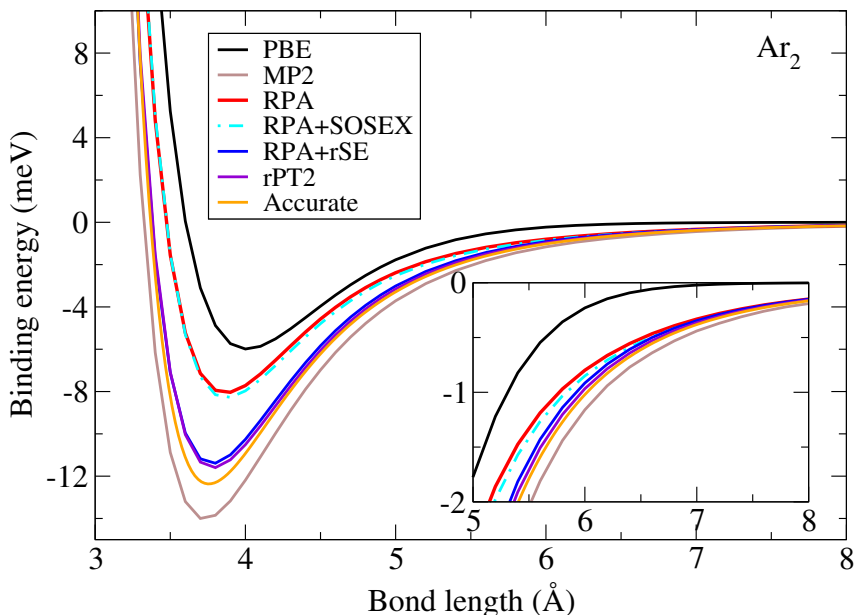
Fig. 2: *Binding energy curves for Ar$_2$ obtained using PBE, MP2, and RPA-based methods. All RPA-based methods use PBE orbitals as input. Calculations are done using the FHI-aims code [75, 74]. The "Accurate" reference curve is given by the Tang-Toennies potential model for Ar$_2$ [80]. The inset is a zoom-in of the asymptotic behavior at large separations.*

improved by RPA. More importantly, at large separations, the PBE binding energy decays rapidly (in fact exponentially) to the energy zero, but the RPA curve displays a correct C_6/R^6 asymptotic behavior. Compared to the reference result, however, the RPA still shows a substantial underbinding behavior, in contrast to the MP2 curve which shows too strong binding of Ar$_2$. The underbinding issue of RPA for vdW dimers arises from the too strong Pauli repulsion, which is in turn due to the Hartree-Fock part of the RPA total energy, obtained with the semi-local GGA orbitals. This issue can be fixed by the single-excitations corrections [17], and in particular its renormalized version [35]. As shown in Fig. 2, the RPA+rSE scheme brings the binding energy curve of Ar$_2$ in close agreement with the reference one. The SOSEX correction, however, does not have a noticeable effect here. Thus the final rPT2 binding energy curve is almost on top of the RPA+rSE one. The performance of RPA-based methods for other rare-gas dimers can be found in Ref. [35].

A widely used benchmark set for weak interactions is the S22 test set designed by Jurečka et al., [82]. This test set collects 22 molecular dimers, among which 7 dimers are of hydrogen binding type, 8 of pure vdW (also called "dispersion") bonding, and another 7 of mixed type. Figure 3(a) shows the structures of water dimer, adenine-thymine dimer, and water-benzene dimer, representing respectively the three bonding types. Because of its good representativity and the availability of accurate reference interaction energies obtained using the CCSD(T) method [81], S22 has been widely used for benchmarking the performance of or training the parameters for computational schemes that aim at describing weak interactions. The performance of RPA and some of the RPA-related methods has been benchmarked for this test set [15, 18, 17, 83].
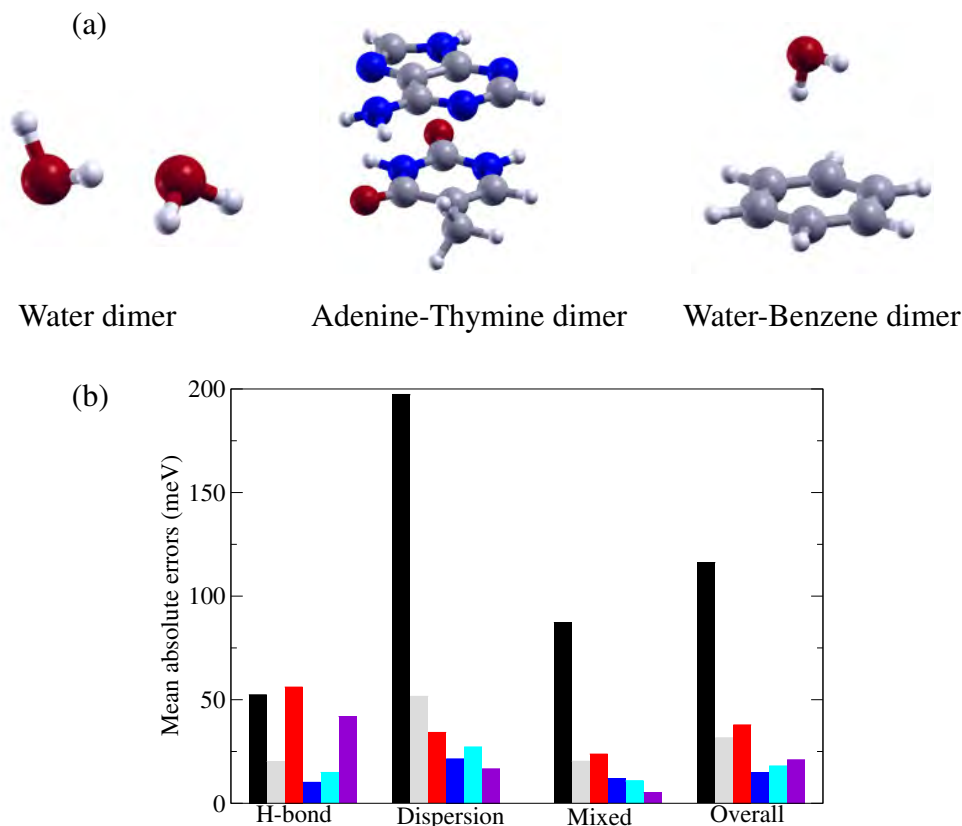
Fig. 3: *(a) Structures of water dimer, adenine-thymine dimer, and water-benzene dimer. C, O, N, and H atoms are represented by grey, red, blue, and white balls. (b) MAEs (in meV) for the S22 test set given by PBE, MP2, RPA, RPA+rSE, RPA+SOSEX, and rPT2 methods. The CCSD(T) results of Takatani et al. [81] are used here as the reference.*

In Fig. 3(b) the mean absolute errors (MAE) of PBE, MP2, and RPA-based methods are presented for the three subsets separately and for the entire S22 set. Both PBE and the correlated methods can describe the hydrogen bonding well, since this type of bonding is dominated by the electrostatic interactions, which has already been captured by the semi-local functionals to a large extent. The error of the standard RPA method is still appreciable (MAE > 1 kcal/mol ≈ 43 meV) arising from its general underbinding behavior. This can again be corrected by rSE, or by SOSEX terms. However, adding the two types of corrections together, the rPT2 scheme tends to overbind the hydrogen-bonded molecules, and hence the MAE increases again. For dispersion and mixed bondings, RPA performs better, and the MAE can be further reduced by rSE and SOSEX corrections. The MP2 method, on the other hand, yields a relatively large MAE for dispersion-bonded molecules, owing to its well-known overbinding problem for this type of interaction. This benchmark test indicates that the RPA+rSE scheme is a suitable approach recommendable for describing weak interactions. The advantage of this scheme is that it does not noticeably increase the computational cost, compared to the standard RPA scheme.

In addition to vdW complexes, RPA and its variants have also been applied to chemically bonded molecules and crystalline solids. Interested readers may look into the literature for further details [21, 84, 37, 35].

4.2   Surface adsorption

An accurate description of atoms and molecules interacting with surfaces is the key to understand important physical and chemical processes such as heterocatalysis, molecular electronics, and corrosion. Molecules adsorbed on metal surfaces represent a particularly difficult situation, since quantitatively accurate results can only be obtained if the approach is able to describe simultaneously the chemical bonding, vdW interactions, metallic screening, and charge transfer processes. The issue is best illustrated by the "CO adsorption puzzle," where LDA and several popular GGAs predict the wrong adsorption site for the CO molecule adsorbed on several noble/transition metal surfaces at low coverages [56]. For CO adsorbed on the Cu(111) or Pt(111) surfaces, LDA and popular GGAs erroneously favor the highly-coordinated hollow site (see, e.g., Fig. 4(a)), whereas experiments clearly show that the singly-coordinated on-top site is the energetically most stable site [85, 86]. This posed a severe challenge to the first-principles modeling of molecular adsorption problems and represents a key test example for the RPA-based methods.

In Ref. [27], the performance of the RPA method for CO adsorbed on Cu(111) was investigated. The computed RPA adsorption energies for both the on-top and fcc (face centered cubic) hollow sites are presented in Fig. 4(b), together with the results from LDA, AM05 [87], PBE, and the hybrid PBE0 functional [88]. Figure 4 reveals what happens in the CO adsorption puzzle when climbing the Jacob's ladder in DFT [9] —going from the first two rungs (LDA and GGAs) to the fourth (hybrid functionals), and finally to the 5th-rung RPA functional. It can be seen that, along the way, the adsorption energies on both sites are reduced, but the magnitude of the reduction is bigger for the fcc hollow site. The correct energy ordering is already restored at the PBE0 level, but the adsorption energy difference between the two sites is vanishingly small. RPA not only predicts the correct adsorption site, but also produces a reasonable adsorption energy difference of 0.22 eV, consistent with experiments. The effect of the starting reference state on the calculated RPA results has also been checked. In Ref. [27], in addition to the commonly used scheme RPA@PBE, RPA calculations were also done on top of the hybrid functional PBE0. Figure 4 indicates that the small difference between RPA@PBE and RPA@PBE0 results is insignificant for understanding the "CO adsorption puzzle."

Schimka *et al.* extended the RPA benchmark studies of the CO adsorption problem to more surfaces [28], and found that RPA is the only approach that gives both good adsorption energies and surface energies. GGAs and hybrid functionals at most yield either good surface energies, or adsorption energies, but not both. Following these works, RPA has subsequently been applied to the adsorption of small alkanes in Na-exchanged chabazite [89], benzene on the Si(001) surface [90], graphene on the Ni(111) surface [29, 30] and the Cu(111) and Co(0001) surfaces [30]. In all these studies, RPA was demonstrated to be able to capture the delicate balance between chemical and dispersion interactions, and yields quantitatively reliable results.

We expect RPA to become an increasingly more important approach in surface science, with increasing computer power and more efficient implementations.

(a)   (b)
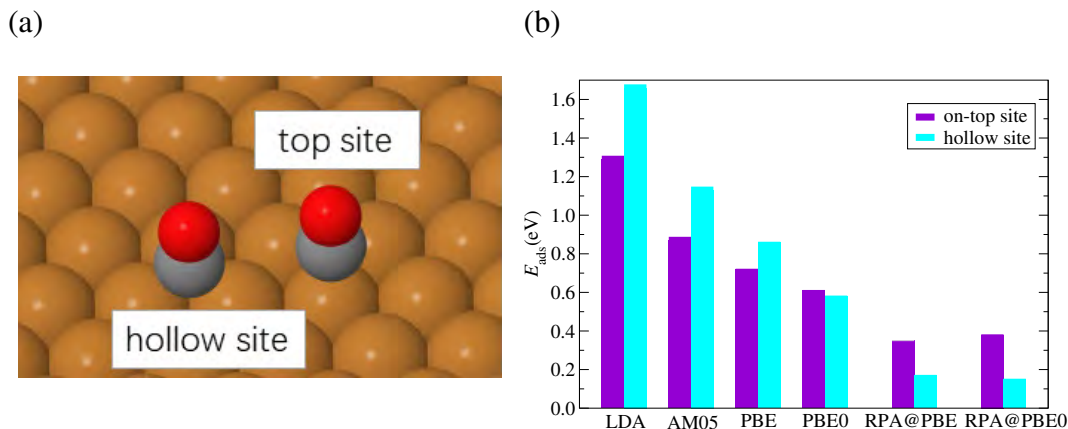
Fig. 4: *(a): Schematic of CO adsorbed on the Cu(111) surface, with the on-top and hollow adsorption sites illustrated. (b): Adsorption energies for CO sitting on the on-top and fcc hollow sites as obtained using LDA, AM05, PBE, PBE0, and RPA. RPA results are presented for both PBE and PBE0 references. Calculations were done with the FHI-aims code. Adopted from Ref. [37].*

4.3   Structural phase transitions

The f-electron materials, which contain rare-earth or actinide elements, pose a great challenge to first-principles approaches. A prominent example of an f-electron system is the Ce metal, which has an intriguing iso-structural α-γ phase transition, accompanied by a drastic volume collapse (as large as 15% at ambient pressure and zero temperature). The two phases are characterized by distinct spectroscopic and magnetic properties. Various theoretical approaches, including LDA plus dynamical mean-field theory (LDA+DMFT) have been employed to study this system [91, 92]. DFT within its local and semilocal approximations is unable to describe the two phases of Ce. In fact, due to the strong delocalization error in these functionals, the localized nature of the f-electrons in the γ phase cannot be properly described; only the α phase is described with some confidence within LDA/GGAs, although not at a quantitative level.

It was shown by Casadei *et al.* [24, 25] that, remarkably, hybrid functionals like PBE0 and HSE can yield two self-consistent solutions, with distinct lattice constants, cohesive energies, electronic band structures, local magnetic moments, and different degrees of f-electron localization. These two solutions can be reasonably associated with the phases of the Ce metal. However, the energetic ordering of the α-like and γ-like phases produced by PBE0 is not consistent with the experimental situation where the α phase is energetically more stable at low temperature and ambient pressure. Adding RPA corrections on top of the PBE cohesive energies for the two solutions, the energy ordering is reversed, and the α-like solution becomes energetically more stable. The transition pressure of the two phases given by the Gibbs construction is consistent with the experimental value.

The capability of RPA to capture the delicate energy difference between competing phases or polymorphs has also been demonstrated for Iron disulfide (FeS$_2$), a potentially interesting system for photovoltaic and photoelectrochemical applications. This material turns out to be rather challenging, since popular conventional density-functional approximations fail to produce the
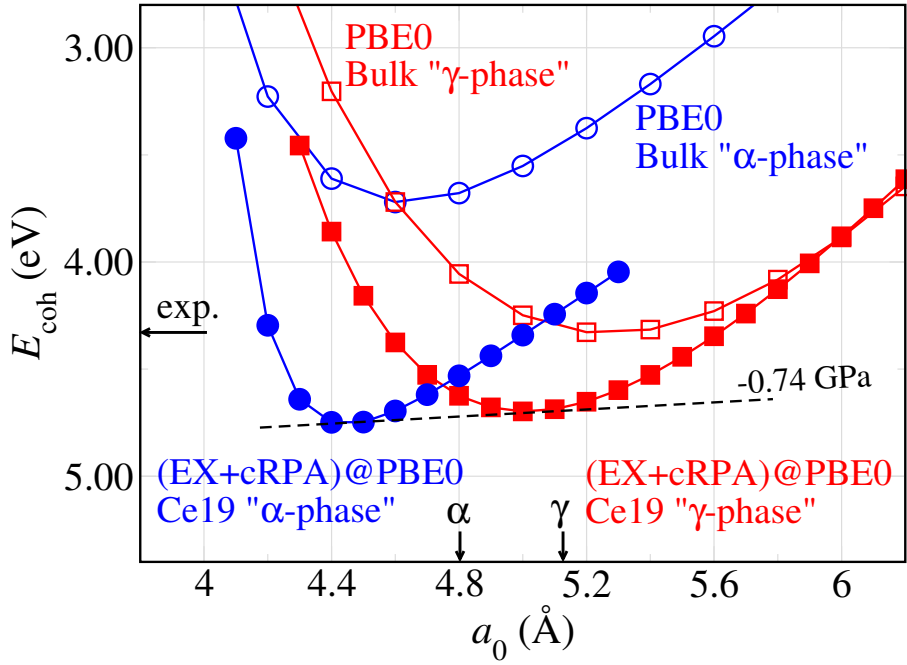
Fig. 5: *Calculated PBE0 and RPA@PBE0 [RPA denoted here as exact-exchange plus RPA correlation (EX+cRPA)] cohesive energy (E_{coh}) as a function of the lattice constant a_0 for the two electronic states based on self-consistent PBE0 solutions. The correction of RPA with respect to the PBE0 cohesive energies was done for a 19-atom fcc-cerium cluster. The dashed line illustrates the Gibbs construction for the transition pressure from the α to the γ phase. The arrows on the energy axes indicates the experimental cohesive energy of the α phase. Adapted from Ref. [24].*

relative stability of its two polymorphs: pyrite and marcasite, with the latter artificially stabilized. It was demonstrated by Zhang *et al.* [26] that RPA, regardless of its reference state, can correctly restore the energy ordering of the two polymorphs of FeS_2. These authors further reveal that the fact that RPA tends to stabilize the pyrite polymorph is due to its smaller KS band gap, resulting in a large RPA correlation energy as compared to the marcasite polymorph. This observation is consistent with the case of the Ce metal [24], where the more metallic α-phase is stabilized within the RPA. Another successful application of this kind is that the tiny energy difference between the two allotropes of carbon, graphite and diamond, can be reliably described by RPA, with the correct prediction that graphite is energetically slightly lower than diamond [31]. More systematic benchmark studies of the performance of RPA and several beyond-RPA methods for predicting the transition pressure of structural phase transitions of a set of bulk materials have recently been reported in Ref. [93].

Other types of materials science problems to which RPA has been applied include layered compounds [94, 36] and defect systems [32, 33]. We shall not elaborate on these types of applications here due to limited space, and interested readers may look into the original literature for details. In summary, there is ample evidence that RPA-based methods perform well in capturing delicate energy differences in materials, and fix some of the qualitative failures of more conventional approaches.

5   Recent developments

The field of RPA-based methodology development and applications represents a rapidly evolving branch of computational electronic structure theory. Notable progress has been achieved in several directions within the last few years, which we would like to briefly recapitulate here.

1. RPA force calculations. Analytical gradients of the RPA total energy with respect to the atomic positions have been computed within both the atomic orbital basis [95–97, 78] and plane-wave basis [98] frameworks. This allows to compute interatomic forces and relax structures at the RPA level, which is a long-sought goal of the electronic-structure community. Moreover, it is now possible to calculate vibrational frequencies [96] and phonon spectra based on the RPA force constant [98], and even molecular dynamics simulations can be carried out based on the RPA forces [98]. These advancements greatly enhanced the capability of RPA in computational chemistry and materials science.

2. Low-scaling RPA implementations. Another noteworthy development is several low-scaling—ranging from linear scaling to cubic scaling—algorithms for RPA calculations have been designed and implemented [99, 100, 33, 101–103]. This paves the way for applying RPA to large-sized and complex materials that were inaccessible in the past.

3. Particle-particle RPA. The above-discussed RPA is represented by ring diagrams and called particle-hole RPA (phRPA) in the literature. In addition to phRPA, another type of RPA, consisting of an infinite summation of ladder diagrams, has also been discussed in the nuclear physics literature [5]. This type of RPA is referred to as particle-particle RPA and has recently been brought to the attention of electronic structure community [104–107]. Benchmark calculations show that ppPRA carries interesting features that are not present in phRPA. Attempts for combining the two types of RPA in one framework have been made both in a range-separated manner [108] and globally [109]. However, it seems that merging the two RPA channels into one united theory is a highly nontrivial task [109].

4. Self-consistent RPA in a generalized Kohn-Sham framework. As mentioned before, the majority of practical RPA calculations are done in a post-processing fashion, using orbitals and orbital energies generated from a preceding DFA calculation. The importance of the rSE contribution indicates that commonly used semi-local DFAs are not optimal starting points for RPA calculations. Thus running RPA calculations in a self-consistent way is highly desirable. However, for orbital-dependent functionals like RPA, the criterion for "self-consistency" is not uniquely defined. The optimized effective potential (OEP) RPA [110–112] is a well-defined procedure, but the obtained results for binding energies are not better than perturbative RPA. Most recently, self-consistent RPA schemes are developed by Jin *et al.* within a generalized OEP framework [113] and by Voora *et al.* within a generalized KS framework [114]. The two schemes differ in details, but the rSE contribution is captured in both schemes. Initial results obtained from these schemes look very promising and there is much to explore along this direction.

5. More beyond-RPA schemes to improve the accuracy. In addition to the beyond-RPA schemes already discussed in Sec. 2.3, one most recent development by Zhang and Xu [115] is to introduce a spin-pair distinctive algorithm in the ACFDT context, whereby the contributions of same-spin and opposite-spin pairs to the correlation energy are separated. By scaling the contributions for two types of spin pairs differently, one can achieve a simultaneous attenuation of both self-interaction errors and static correlation errors. Similar to the power series approximation of Görling and coauthors [62,59], the spin-pair distinctive formalism of Zhang and Xu [115] is particularly successful in dealing with systems with multi-reference characters.

6   Summary

In this lecture, we discussed the basic concept, the theoretical formulation, the implementation algorithm, the prototypical applications, and the recent development of RPA-based methods. We expect that RPA and its variants will have an ever-increasing impact on computational materials science, and become the mainstream methods in the near future. Since this is an actively developing field, and the number of papers is quickly growing, it is well possible some important developments are not covered in our discussion. The purpose of this manuscript is to inform the readers about the overall status of this field, and stimulate more work on the development and application of RPA-type methodology.

Acknowledgements

References

[1] D. Bohm and D. Pines, Phys. Rev. **82**, 625 (1951)

[2] D. Bohm and D. Pines, Phys. Rev. **92**, 609 (1953)

[3] J. Hubbard, Proc. Roy. Soc. (London) **A240**, 539 (1957)

[4] M. Gell-Mann and K.A. Brueckner, Phys. Rev. **106**, 364 (1957)

[5] P. Ring and P. Schuck: *The Nuclear Many-Body Problem* (Springer, New York, 1980)

[6] D.C. Langreth and J.P. Perdew, Solid State Commun. **17**, 1425 (1975)

[7] D.C. Langreth and J.P. Perdew, Phys. Rev. B **15**, 2884 (1977)

[8] O. Gunnarsson and B.I. Lundqvist, Phys. Rev. B **13**, 4274 (1976)

[9] J.P. Perdew and K. Schmidt, in V. Van Doren, C. Van Alsenoy, and P. Geerlings (eds.):
Density Functional Theory and its Application to Materials (AIP, Melville, NY, 2001)

[10] F. Furche, Phys. Rev. B **64**, 195120 (2001)

[11] M. Fuchs and X. Gonze, Phys. Rev. B **65**, 235109 (2002)

[12] H. Jiang and E. Engel, J. Chem. Phys **127**, 184108 (2007)

[13] M. Hellgren and U. von Barth, Phys. Rev. B **76**, 075107 (2007)

[14] J. Toulouse, I.C. Gerber, G. Jansen, A. Savin, and J.G. Ángyán,
Phys. Rev. Lett. **102**, 096404 (2009)

[15] W. Zhu, J. Toulouse, A. Savin, and J.G. Ángyán, J. Chem. Phys. **132**, 244108 (2010)

[16] A. Heßelmann and A. Görling, Phys. Rev. Lett. **106**, 093001 (2011)

[17] X. Ren, A. Tkatchenko, P. Rinke, and M. Scheffler, Phys. Rev. Lett. **106**, 153003 (2011)

[18] H. Eshuis and F. Furche, J. Phys. Chem. Lett. **2**, 983 (2011)

[19] J. Harl and G. Kresse, Phys. Rev. B **77**, 045136 (2008)

[20] J. Harl and G. Kresse, Phys. Rev. Lett. **103**, 056401 (2009)

[21] J. Harl, L. Schimka, and G. Kresse, Phys. Rev. B **81**, 115126 (2010)

[22] H.V. Nguyen and S. de Gironcoli, Phys. Rev. B **79**, 205114 (2009)

[23] D. Lu, Y. Li, D. Rocca, and G. Galli, Phys. Rev. Lett. **102**, 206411 (2009)

[24] M. Casadei, X. Ren, P. Rinke, A. Rubio, and M. Scheffler,
Phys. Rev. Lett. **109**, 146402 (2012)

[25] M. Casadei, X. Ren, P. Rinke, A. Rubio, and M. Scheffler,
Phys. Rev. B **93**, 075153 (2016)

[26] M.Y. Zhang, Z.H. Cui, and H. Jiang, J. Mater. Chem. A **6**, 6606 (2018)

[27] X. Ren, P. Rinke, and M. Scheffler, Phys. Rev. B **80**, 045402 (2009)

[28] L. Schimka, J. Harl, A. Stroppa, A. Grüneis, M. Marsman, F. Mittendorfer,
and G. Kresse, Nat. Mater. **9**, 741 (2010)

[29] F. Mittendorfer, A. Garhofer, J. Redinger, J. Klimeš, J. Harl, and G. Kresse,
Phys Rev. B **84**, 201401(R) (2011)

[30] T. Olsen, J. Yan, J.J. Mortensen, and K.S. Thygesen, Phys. Rev. Lett. **107** (2011)

[31] S. Lebègue, J. Harl, T. Gould, J.G. Ángyán, G. Kresse, and J.F. Dobson,
Phys. Rev. Lett. **105**, 196401 (2010)

[32] F. Bruneval, Phys. Rev. Lett. **108**, 256403 (2012)

[33] M. Kaltak, J. Klimeš, and G. Kresse, J. Chem. Theory Comput. **10**, 2498 (2014)

[34] J.F. Dobson, A. White, and A. Rubio, Phys. Rev. Lett. **96**, 073201 (2006)

[35] X. Ren, P. Rinke, G.E. Scuseria, and M. Scheffler, Phys. Rev. B **88**, 035120 (2013)

[36] T. Björkman, A. Gulans, A.V. Krasheninnikov, and R.M. Nieminen,
Phys. Rev. Lett. **108**, 235502 (2012)

[37] X. Ren, P. Rinke, C. Joas, and M. Scheffler, J. Mater. Sci. **47**, 7447 (2012)

[38] D. Pines, Rep. Prog. Phys. **79**, 092501 (2016)

[39] G.P. Chen, V.K. Voora, M.M. Agee, S.G. Balasubramani, and F. Furche,
Annu. Rev. Phys. Chem. **68**, 421 (2017)

[40] R.J. Bartlett and M. Musiał, Rev. Mod. Phys. **79**, 291 (2007)

[41] G.E. Scuseria, T.M. Henderson, and D.C. Sorensen, J. Chem. Phys. **129**, 231101 (2008)

[42] N.E. Dahlen, R. van Leeuwen, and U. von Barth, Phys. Rev. A **73**, 012511 (2006)

[43] F. Caruso, D.R. Rohr, M. Hellgren, X. Ren, P. Rinke, A. Rubio, and M. Scheffler,
Phys. Rev. Lett. **110**, 146403 (2013)

[44] W. Kohn and L.J. Sham, Phys. Rev. **140**, A1133 (1965)

[45] A. Becke, J. Chem. Phys. **88**, 2547 (1988)

[46] C. Lee, W. Yang, and R.G. Parr, Phys. Rev. B **37**, 785 (1988)

[47] J.P. Perdew, K. Burke, and M. Ernzerhof, Phys. Rev. Lett. **77**, 3865 (1996)

[48] J. Tao, J.P. Perdew, V.N. Staroverov, and G.E. Scuseria,
     Phys. Rev. Lett. **91**, 146401 (2003)

[49] J. Sun, A. Ruzsinszky, and J.P. Perdew, Phys. Rev. Lett. **115**, 036402 (2015)

[50] A.D. Becke, J. Chem. Phys **98**, 5648 (1993)

[51] J. Heyd, G.E. Scuseria, and M. Ernzerhof, J. Chem. Phys. **118**, 8207 (2003)

[52] J.P. Perdew, R.G. Parr, M. Levy, and J.L. Balduz, Jr., Phys. Rev. Lett. **49**, 1691 (1982)

[53] A.J. Cohen, P. Mori-Sanchez, and W. Yang, Science **321**, 792 (2008)

[54] S. Kristyán and P. Pulay, Chem. Phys. Lett. **229**, 175 (1994)

[55] M. Imada, A. Fujimori, and Y. Tokura, Rev. Mol. Phys. **70**, 1039 (1998)

[56] P.J. Feibelman, B. Hammer, J.K. Nørskov, F. Wagner, M. Scheffler, R. Stumpf, R. Watwe,
     and J. Dumestic, J. Phys. Chem. B **105**, 4018 (2001)

[57] Y. Zhang and W. Yang, J. Chem. Phys. **109**, 2604 (1998)

[58] P. Nozières and D. Pines: *The Theory of Quantum Liquids* (Benjamin, New York, 1966)

[59] A. Görling, Phys. Rev. B **99**, 235120 (2019)

[60] A. Ruzsinszky, J.P. Perdew, and G.I. Csonka, J. Chem. Theory Comput. **6**, 127 (2010)

[61] T. Olsen and K.S. Thygesen, Phys. Rev. B **86**, 081103(R) (2012)

[62] J. Erhard, P. Bleizier, and A. Görling, Phys. Rev. Lett. **117**, 143002 (2016)

[63] D.L. Freeman, Phys. Rev. B **15**, 5512 (1977)

[64] A. Grüneis, M. Marsman, J. Harl, L. Schimka, and G. Kresse,
     J. Chem. Phys. **131**, 154115 (2009)

[65] J. Paier, B.G. Janesko, T.M. Henderson, G.E. Scuseria, A. Grüneis, and G. Kresse,
     J. Chem. Phys. **132**, 094103 (2010); Erratum: *ibid.* **133**, 179902 (2010)

[66] A. Szabo and N.S. Ostlund: *Modern Quantum Chemistry:*
     Introduction to Advanced Electronic Structure Theory (McGraw-Hill, New York, 1989)

[67] J.E. Bates and F. Furche, J. Chem. Phys. **139**, 171103 (2013)

[68] G.P. Chen, M.M. Agee, and F. Furche, J. Chem. Theory Comput. **14**, 5701 (2018)

[69] M.J. Frisch *et al.*: *Gaussian 09W Revision D.01*. Gaussian Inc. Wallingford CT 2009

[70] *TURBOMOLE V7.3 2018, a development of University of Karlsruhe and Forschungszen-*
     trum Karlsruhe GmbH, 1989-2007, TURBOMOLE GmbH, since 2007; available from
     `http://www.turbomole.com`.

[71] J. Paier, M. Marsman, K. Hummer, G. Kresse, I.C. Gerber, and J.G. Ángyán,
     J. Chem. Phys. **124**, 154709 (2006)

[72] S.V. Levchenko, X. Ren, J. Wieferink, R. Johanni, P. Rinke, V. Blum, and M. Scheffler,
     Comp. Phys. Comm. **192**, 60 (2015)

[73] H. Eshuis, J. Yarkony, and F. Furche, J. Chem. Phys. **132**, 234114 (2010)

[74] X. Ren, P. Rinke, V. Blum, J. Wieferink, A. Tkatchenko, A. Sanfilippo, K. Reuter,
     and M. Scheffler, New J. Phys. **14**, 053020 (2012)

[75] V. Blum, F. Hanke, R. Gehrke, P. Havu, V. Havu, X. Ren, K. Reuter, and M. Scheffler,
     Comp. Phys. Comm. **180**, 2175 (2009)

[76] A.C. Ihrig, J. Wieferink, I.Y. Zhang, M. Ropo, X. Ren, P. Rinke, M. Scheffler,
     and V. Blum, New J. Phys. **17**, 093020 (2015)

[77] O. Vahtras, J. Almlöf, and M.W. Feyereisen, Chem. Phys. Lett. **213**, 514 (1993)

[78] M. Beuerle and C. Ochsenfeld, J. Chem. Phys. **149**, 244111 (2018)

[79] J.F. Dobson, in M.P. Das (ed.): *Topics in Condensed Matter Physics*
     (Nova, New York, 1994)

[80] K.T. Tang and J.P. Toennies, J. Chem. Phys. **118**, 4976 (2003)

[81] T. Takatani, E.G. Hohenstein, M. Malagoli, M.S. Marshall, and C.D. Sherrill,
     J. Chem. Phys. **132**, 144104 (2010)

[82] P. Jurečka, J. Šponer, J. Černý, and P. Hobza, Phys. Chem. Chem. Phys. **8**, 1985 (2006)

[83] H. Eshuis and F. Furche, J. Chem. Phys. **136**, 084105 (2012)

[84] J. Paier, X. Ren, P. Rinke, G.E. Scuseria, A. Grüneis, G. Kresse, and M. Scheffler,
     New J. Phys. **14**, 043002 (2012)

[85] H. Steininger, S. Lehwald, and H. Ibach, Surf. Sci. **123**, 264 (1982)

[86] G.S. Blackman, M.L. Xu, D.F. Ogletree, M.A.V. Hove, and G.A. Somorjai,
     Phys. Rev. Lett. **61**, 2352 (1988)

[87] R. Armiento and A.E. Mattsson, Phys. Rev. B **72**, 085108 (2005)

[88] J.P. Perdew, M. Ernzerhof, and K. Burke, J. Chem. Phys. **105**, 9982 (1996)

[89] F. Göltl and J. Hafner, J. Chem. Phys. **134**, 064102 (2011)

[90] H.J. Kim, A. Tkatchenko, J.H. Cho, and M. Scheffler, Phys. Rev. B **85**, 041403 (2012)

[91] K. Held, A. McMahan, and R. Scalettar, Phys. Rev. Lett. **87**, 1 (2001)

[92] B. Amadon, S. Biermann, A. Georges, and F. Aryasetiawan, Phys. Rev. Lett. **96**, 1 (2006)

[93] N. Sengupta, J.E. Bates, and A. Ruzsinszky, Phys. Rev. B **97**, 235136 (2018)

[94] A. Marini, P. García-González, and A. Rubio, Phys. Rev. Lett **96**, 136404 (2006)

[95] J. Rekkedal, S. Coriani, M.F. Iozzi, A.M. Teale, T. Helgaker, and T.B. Pedersen,
      J. Chem. Phys. **139**, 081101 (2013)

[96] A.M. Burow, J.E. Bates, F. Furche, and H. Eshuis,
      J. Chem. Theory Comput. **10**, 180 (2014)

[97] B. Mussard, P.G. Szalay, and J.G. Ángyán, J. Chem. Theory. Comput. **10**, 1968 (2014)

[98] B. Ramberger, T. Schäfer, and G. Kresse, Phys. Rev. Lett. **118**, 106403 (2017)

[99] D. Neuhauser, E. Rabani, and R. Baer, J. Phys. Chem. Lett. **4**, 1172 (2013)

[100] J.E. Moussa, J. Chem. Phys. **140**, 014107 (2014)

[101] M. Kállay, J. Chem. Phys. **142**, 204105 (2015)

[102] J. Wilhelm, P. Seewald, M. Del Ben, and J. Hutter,
      J. Chem. Theory Comput. **12**, 5851 (2016)

[103] D. Graf, M. Beuerle, H.F. Schurkus, A. Luenser, G. Savasci, and C. Ochsenfeld,
      J. Chem. Theory Comput. **14**, 2505 (2018)

[104] H. van Aggelen, S.N. Steinmann, D. Peng, and W. Yang,
      Phys. Rev. A **88**, 030501(R) (2013)

[105] D. Peng, S.N. Steinmann, H. van Aggelen, and W. Yang,
      J. Chem. Phys. **139**, 103112 (2013)

[106] Y. Yang, H. van Aggelen, S.N. Steinmann, D. Peng, and W. Yang,
      J. Chem. Phys. **139**, 174110 (2013)

[107] E. Scuseria, T.M. Henderson, and I.W. Bulik, J. Chem. Phys. **139**, 104113 (2013)

[108] J.J. Shepherd, T.M. Henderson, and G.E. Scuseria, Phys. Rev. Lett. **112**, 133002 (2014)

[109] M.N. Tahir and X. Ren, Phys. Rev. B **99**, 195149 (2019)

[110] P. Verma and R.J. Bartlett, The Journal of Chemical Physics **136**, 044105 (2012)

[111] P. Bleiziffer, A. Hesselmann, and A. Görling, J. Chem. Phys. **139**, 084113 (2013)

[112] M. Hellgren, F. Caruso, D.R. Rohr, X. Ren, A. Rubio, M. Scheffler, and P. Rinke,
      Phys. Rev. B **91**, 165110 (2015)

[113] Y. Jin, D. Zhang, Z. Chen, N.Q. Su, and W. Yang, J. Phys. Chem. Lett. **8**, 4746 (2017)

[114] V.K. Voora, S.G. Balasubramani, and F. Furche, Phys. Rev. A **99**, 012518 (2019)

[115] I.Y. Zhang and X. Xu, J. Phys. Chem. Lett. **10**, 2617 (2019)